



## A model of the magnetosheath magnetic field during magnetic clouds

Lucile Turc, Dominique Fontaine, Philippe Savoini, E.K.J. Kilpua

### ► To cite this version:

Lucile Turc, Dominique Fontaine, Philippe Savoini, E.K.J. Kilpua. A model of the magnetosheath magnetic field during magnetic clouds. *Annales Geophysicae*, 2014, 32 (2), pp.157-173. 10.5194/angeo-32-157-2014 . hal-01307422

**HAL Id: hal-01307422**

**<https://hal.sorbonne-universite.fr/hal-01307422>**

Submitted on 26 Apr 2016

**HAL** is a multi-disciplinary open access archive for the deposit and dissemination of scientific research documents, whether they are published or not. The documents may come from teaching and research institutions in France or abroad, or from public or private research centers.

L'archive ouverte pluridisciplinaire **HAL**, est destinée au dépôt et à la diffusion de documents scientifiques de niveau recherche, publiés ou non, émanant des établissements d'enseignement et de recherche français ou étrangers, des laboratoires publics ou privés.



Distributed under a Creative Commons Attribution| 4.0 International License



# A model of the magnetosheath magnetic field during magnetic clouds

L. Turc<sup>1</sup>, D. Fontaine<sup>1</sup>, P. Savoini<sup>1</sup>, and E. K. J. Kilpua<sup>2</sup>

<sup>1</sup>Ecole Polytechnique, CNRS, Sorbonne Universités, UPMC Univ Paris 06, Univ Paris-Sud, UMR7648, Laboratoire de Physique des Plasmas, 91128, Palaiseau, France

<sup>2</sup>Department of Physics, University of Helsinki, P.O. Box 64, 00014 Helsinki, Finland

Correspondence to: L. Turc (lucile.turc@lpp.polytechnique.fr)

Received: 14 November 2013 – Revised: 16 January 2014 – Accepted: 17 January 2014 – Published: 21 February 2014

**Abstract.** Magnetic clouds (MCs) are huge interplanetary structures which originate from the Sun and have a paramount importance in driving magnetospheric storms. Before reaching the magnetosphere, MCs interact with the Earth's bow shock. This may alter their structure and therefore modify their expected geoeffectivity. We develop a simple 3-D model of the magnetosheath adapted to MCs conditions. This model is the first to describe the interaction of MCs with the bow shock and their propagation inside the magnetosheath. We find that when the MC encounters the Earth centrally and with its axis perpendicular to the Sun–Earth line, the MC's magnetic structure remains mostly unchanged from the solar wind to the magnetosheath. In this case, the entire dayside magnetosheath is located downstream of a quasi-perpendicular bow shock. When the MC is encountered far from its centre, or when its axis has a large tilt towards the ecliptic plane, the MC's structure downstream of the bow shock differs significantly from that upstream. Moreover, the MC's structure also differs from one region of the magnetosheath to another and these differences vary with time and space as the MC passes by. In these cases, the bow shock configuration is mainly quasi-parallel. Strong magnetic field asymmetries arise in the magnetosheath; the sign of the magnetic field north–south component may change from the solar wind to some parts of the magnetosheath. We stress the importance of the  $B_x$  component. We estimate the regions where the magnetosheath and magnetospheric magnetic fields are anti-parallel at the magnetopause (i.e. favourable to reconnection). We find that the location of anti-parallel fields varies with time as the MCs move past Earth's environment, and that they may be situated near the subsolar region even for an initially northward

magnetic field upstream of the bow shock. Our results point out the major role played by the bow shock configuration in modifying or keeping the structure of the MCs unchanged. Note that this model is not restricted to MCs, it can be used to describe the magnetosheath magnetic field under an arbitrary slowly varying interplanetary magnetic field.

**Keywords.** Magnetospheric physics (magnetosheath; solar-wind–magnetosphere interactions)

## 1 Introduction

Coronal mass ejections (CMEs) are huge blobs of plasma released from the solar corona during eruptive events. They travel into the heliosphere, where they are called interplanetary coronal mass ejections (ICMEs) and, if they are Earth-directed, interact with the terrestrial environment. Many statistical studies point out the major role played by ICMEs in driving geomagnetic storms, especially during solar maximum (Richardson et al., 2001, 2002; Echer et al., 2008; Yermolaev et al., 2012). Around one third of the ICMEs observed in the vicinity of Earth exhibit magnetic cloud (MC) signatures (Richardson and Cane, 2010). MCs are characterised by a magnetic field strength higher than that in the ambient solar wind, a smooth and long-lasting rotation of the magnetic field direction, and a low proton temperature (Burlaga et al., 1981). Due to their slowly rotating magnetic field, MCs can contain long periods of southward magnetic fields which are expected to reconnect with Earth's dipolar field at the magnetopause and cause intense storms (see, for example, Zhang et al., 2004; Huttunen et al., 2005).

However, the accuracy of predicting the level of geomagnetic disturbances from the solar wind parameters is still rather modest (see, for example, Chen et al., 2012, and the references therein). The geoeffectivity or lack of geoeffectivity of an MC is not related at 100 % to the southward or northward orientation of its magnetic field. Some MCs containing southward fields do not trigger geomagnetic activity (Zhang et al., 2004; Gopalswamy et al., 2008). The events with only northward fields are more complex and more rarely observed; such storms are generally associated with the sheath region of the MC (Huttunen et al., 2005; Gopalswamy et al., 2008). It has been suggested that the magnetosheath would have a key role in controlling the solar-wind–magnetosphere coupling (e.g. Šafránková et al., 2009).

Before reaching the magnetosphere, the solar wind passes through the bow shock into the magnetosheath. This transition modifies the solar wind properties, and presumably the MCs' structure. It should be noted that it is ultimately the magnetosheath plasma and magnetic field which interact with the magnetopause and determine the geomagnetic response. The measurements inside the magnetosheath are sporadic, and thus the modifications of the structures from the solar wind to the magnetosheath are not well known. This limited understanding may be the key to improve solar-wind–magnetosphere coupling functions and our ability to forecast space weather consequences of MCs.

The plasma flow pattern in the magnetosheath is rather complex. The solar wind is deflected around the magnetosphere and re-accelerates at the flanks. Observations indicate the presence of dawn–dusk asymmetries in the magnetosheath speed (Longmore et al., 2005; Walsh et al., 2012). The properties of the magnetosheath during low Alfvén Mach number ( $M_A$ ) solar wind, corresponding to ICMEs and MCs conditions, have been investigated both observationally and numerically in Lavraud and Borovsky (2008) and Lavraud et al. (2013). Their results show that the solar-wind–magnetosphere coupling is altered in low  $M_A$  conditions, and phenomena such as asymmetric and enhanced flows or asymmetric magnetopause compression are observed.

In terms of the magnetic field, several processes come into play inside the magnetosheath. First, the bow shock crossing alters the interplanetary magnetic field (IMF) strength and direction, according to the Rankine–Hugoniot conservation laws. Then, as the flow is deflected around the magnetosphere, the magnetic field lines, which are frozen into the plasma, are consequently distorted. This phenomenon is known as the draping of the field lines. Statistical studies carried out by Coleman (2005) and Longmore et al. (2006) show that the orientation of the magnetic field in the plane perpendicular to the Sun–Earth line (i.e. the clock angle) differs significantly in the magnetosheath from that observed in the solar wind. Longmore et al. (2006) stress the role played by field–flow coupling in determining the distortion of the field lines inside the magnetosheath.

Discrepancies between the orientation of the magnetosheath magnetic field and the IMF are also evidenced by Šafránková et al. (2009). Using simultaneous solar wind and magnetosheath observations, Šafránková et al. (2009) compare the sign of the magnetic field north–south ( $B_z$ ) component in both regions. Statistically, the probability of observation of the same  $B_z$  sign in the magnetosheath and in the solar wind is rarely close to 1. This probability decreases with  $|B_z|$ , and is around 0.5 (i.e. a random coincidence) for small  $B_z$  values.

In the case of MCs, the magnetic structure observed in the upstream solar wind is well defined and slowly varying. But downstream of the bow shock, their smoothly rotating structure may be altered. Moreover, the magnetosheath magnetic field depends on the location inside this region because of the draping of the field lines, the dawn–dusk asymmetries and the different shock configurations. Spacecraft provide in situ observations along their orbit, but as mentioned above their coverage of the magnetosheath is limited. A magnetosheath model is thus necessary to have a global view of how MCs interact with the bow shock and how their structure changes from the solar wind to the magnetosheath. To our knowledge, there is neither a modelling nor an observational study addressing this question.

In this paper, we build a simple 3-D model describing the interaction of an MC with Earth's bow shock and its propagation into the magnetosheath. We do not intend to describe all the details of this complicated interaction. This work rather highlights the main features of this interaction, in order to pave the way for more comprehensive studies. The model is described in Sect. 2. We validate its outputs in Sect. 3. The results for different orientations of the MC's axis and different impact parameters are provided in Sect. 4 and their consequences on the MCs' geoeffectivity are discussed in Sect. 5. Section 6 concludes the paper with a summary and a discussion of our findings.

## 2 Magnetosheath model

The solar wind flow around the magnetic obstacle formed by the magnetosphere is often determined by solving the gas-dynamic equations for a non-magnetised flow. The widely used hydrodynamic model of Spreiter et al. (1966) has been largely tested over the years and has shown good agreement with spacecraft observations (see, for example, the review by Stahara, 2002). However, the computational cost of this model is rather high, since the equations of gasdynamics have to be solved in the entire simulation grid.

Analytical or semi-empirical magnetosheath models have also been developed, aiming at describing the magnetosheath flow or magnetic field with a limited set of equations. The Russell et al. (1983) model introduces an analytical formula to calculate the magnetosheath streamlines and relate magnetosheath phenomena to the conditions at the bow shock. The

Kobel and Flückiger (1994) model determines the steady-state magnetosheath magnetic field, assuming that the currents are confined at the bow shock and at the magnetopause and that the magnetosheath can be considered as a current-free region. With this hypothesis, the magnetic field can be reduced to a scalar potential, satisfying the Laplace equation. As mentioned by the authors and recently applied and extended by Génot et al. (2011), this model can be used to trace the flowline pattern in the magnetosheath. Kallio and Koskinen (2000) have developed a semi-empirical model of the magnetosheath velocity and magnetic field, which requires a specific magnetospheric field model. The functional form and the free parameters of this model have been adjusted to match global fluid simulation results. More recently, Romashets et al. (2008) introduced an analytical model of the magnetic field based on the boundary conditions imposed by the bow shock and the magnetopause. These three magnetic field models (Kobel and Flückiger, 1994; Kallio and Koskinen, 2000; Romashets et al., 2008) are formulated in parabolic coordinates, and the bow shock and magnetopause shapes are prescribed to be paraboloids, generally with the same focus. Soucek and Escoubet (2012) recently introduced a method extending the applicability of the Kobel and Flückiger (1994) model to any magnetopause model and to any parabolic bow shock model.

In this study, we will use the Soucek and Escoubet (2012) model to describe the flowline pattern in the magnetosheath because of its low computational cost and the absence of strong constraints on the magnetopause and bow shock shapes. The flowline determination, the magnetic field propagation method and the inputs of our model are detailed in the following sections. Our model is formulated in Geocentric Solar Ecliptic (GSE) coordinates and all quantities will be given in this frame.

## 2.1 Boundaries

To apply the Soucek and Escoubet (2012) magnetosheath model, we need to approximate the bow shock and magnetopause shapes. Over the past decades, many different bow shock models have been developed, on the basis of observed bow shock crossings, magnetohydrodynamic (MHD) considerations or simulation results (see, for example, the review by Měrka et al. (2003), and the references therein). In most cases, the bow shock shape and position are parametrised by the upstream solar wind dynamic pressure and Mach number, either sonic (Spreiter et al., 1966), magnetosonic (Farris and Russell, 1994) or Alfvénic (Jeřáb et al., 2005). The bow shock models are generally optimised for high Mach numbers, corresponding to the most commonly encountered solar wind conditions. However, because of their high magnetic field magnitude and rather low density, MCs are characterised by a low Alfvén Mach number ( $M_A$ ). In a comparative study of the predictive capabilities of four different bow

shock models, Turc et al. (2013) concluded that the Jeřáb et al. (2005) model was the most reliable in MC conditions.

In our magnetosheath model, we will use the Jeřáb et al. (2005) bow shock model, which requires the solar wind  $M_A$ , dynamic pressure and magnetic field strength as inputs. The magnetopause will be described by the widely used Shue et al. (1998) model, which is valid even during extreme solar wind conditions. This model depends on the IMF north–south component and the solar wind dynamic pressure.

## 2.2 Flowlines

The flowlines are determined with the Soucek and Escoubet (2012) magnetosheath flow model, in which the flowline pattern is calculated with the Kobel and Flückiger (1994) model and then modified to fit the chosen boundaries. The bow shock and magnetopause shapes calculated from the Jeřáb et al. (2005) and Shue et al. (1998) models, respectively, are depicted in Fig. 1 (red and blue solid lines), for the following upstream solar wind conditions:  $V_{SW} = 400 \text{ km s}^{-1}$ ,  $n_{SW} = 5 \text{ cm}^{-3}$ ,  $M_A = 4.1$  and  $B_z = -10 \text{ nT}$  (the magnetic field is assumed to be purely southward). The Kobel and Flückiger (1994) parabolic boundary corresponding to the Jeřáb et al. (2005) bow shock is indicated by the red dashed line. It is in a very good agreement with the Jeřáb et al. (2005) model on the dayside ( $x \geq 0$ ). The dashed blue line shows the magnetopause in the Kobel and Flückiger (1994) model associated with their parabolic bow shock (in red). Between these boundaries, the flowlines can be computed analytically (dashed black lines). However, the shape of the magnetosheath in the Kobel and Flückiger (1994) model differs largely from that delineated by the Jeřáb et al. (2005) and Shue et al. (1998) models. This limitation can be circumvented using the Soucek and Escoubet (2012) rescaling method.

The flowline pattern is determined in two steps. First, the flowlines are analytically calculated in the magnetosheath bounded by the Kobel and Flückiger (1994) magnetopause and bow shock. Then these flowlines are rescaled to fit the chosen boundaries, that is, the Shue et al. (1998) (solid blue line) and the Jeřáb et al. (2005) (solid red line) models (see Soucek and Escoubet, 2012, for more detail). Figure 1 shows five example flowlines in the Kobel and Flückiger (1994) magnetosheath (dashed black lines) and their rescaled counterparts in the magnetosheath between the chosen boundaries (solid black lines) from the same starting point at the bow shock.

To determine the magnitude of the flow velocity, we have to assume a density profile inside the magnetosheath. Similarly to Soucek and Escoubet (2012) and Génot et al. (2011), we use a crude density profile defined as follows: the ratio between the density  $\rho$  at a fractional distance  $F$  and the density just downstream of the shock  $\rho_d$  is given by  $\rho/\rho_d = 0.8 + 0.2 \times \tanh(4F)$ .

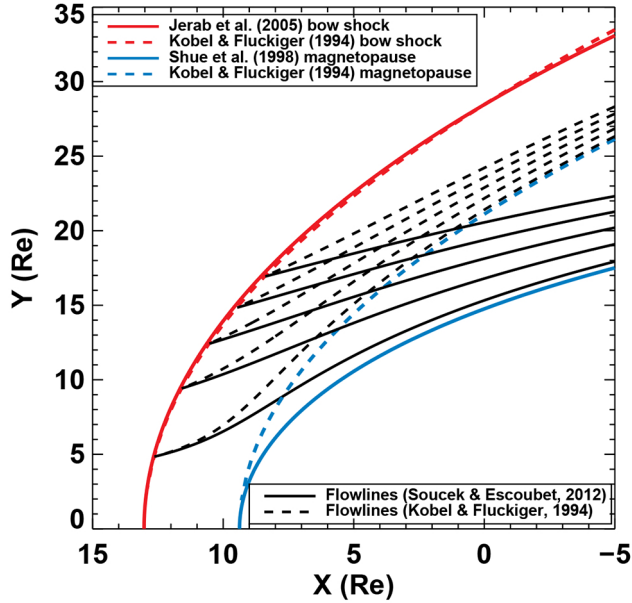


**Fig. 1.** Boundaries: Jeřáb et al. (2005) bow shock model (solid red line), Kobel and Flückiger (1994) bow shock model (dashed red line), Shue et al. (1998) magnetopause model (solid blue line), Kobel and Flückiger (1994) magnetopause model (dashed blue line) – Flowlines in the magnetosheath: in the Soucek and Escoubet (2012) model (solid black lines) and in the Kobel and Flückiger (1994) model (dashed black lines)

### 2.3 Magnetic field propagation

MCs can contain very strong currents, causing their spiralling magnetic field, which will most likely be transmitted into the magnetosheath. Therefore, we cannot use the Kobel and Flückiger (1994) magnetic field model which assumes that the magnetosheath magnetic field is curl free (i.e. that there is no current in this region). Thus the magnetic field is propagated inside the magnetosheath assuming that the plasma in this region can be described with ideal MHD (i.e. the magnetic field lines are frozen into the plasma).

The propagation of the magnetic field is based on the following equations:

$$\nabla \cdot \mathbf{B} = 0 \quad (1)$$

$$\nabla \times \mathbf{E} = -\partial \mathbf{B} / \partial t \quad (2)$$

$$\mathbf{E} + \mathbf{V} \times \mathbf{B} = 0. \quad (3)$$

Combining Eqs. (1), (2) and (3) yields that the variation of the magnetic field can be written as

$$\partial \mathbf{B} / \partial t + (\mathbf{V} \cdot \nabla) \mathbf{B} = (\mathbf{B} \cdot \nabla) \mathbf{V} - \mathbf{B} (\nabla \cdot \mathbf{V}). \quad (4)$$

The magnetic field is then calculated step by step along the flowline from its origin at the bow shock to a given grid point inside the magnetosheath with Eq. (4). Moreover, we require that  $\mathbf{B}$  remains divergence free during its propagation (i.e. Eq. (1) must be satisfied at each step).

### 2.4 Model inputs

The inputs of the magnetosheath model are synthetic solar wind parameters upstream of the bow shock. The MC is assumed to have a force-free flux rope geometry with constant  $\alpha$  (Burlaga, 1988), that is, the magnetic field satisfies the equation:  $\nabla \times \mathbf{B} = \alpha \mathbf{B}$ . Moreover, we assume that the MC presents a cylindrical symmetry about its central axis. In a cylindrical frame centred on the MC axis, with  $A$  being the axis direction,  $R$  the radial direction and  $T$  the tangential direction, the magnetic field components inside the MC are given by

$$B_A = B_0 J_0(ar) \quad (5)$$

$$B_R = 0 \quad (6)$$

$$B_T = B_0 H J_1(ar), \quad (7)$$

where  $J_0$  and  $J_1$  are the zeroth and first order Bessel functions,  $r$  the distance from the axis,  $a$  a constant and  $H = \pm 1$  the handedness of the MC.  $B_0$  is a constant corresponding to the MC's axial magnetic field. In the following, its value is set to  $\pm 20$  nT. Its magnitude is chosen on the basis of the observations, as the average peak magnetic field strength observed at variable distances from the MC's axis ranges between 16 and 18 nT (Echer et al., 2005; Wu and Lepping, 2011). Since the average duration of an MC passing by the Earth is about one day (Lepping et al., 2006), the radius of the MC  $R_{\max}$  is taken to be 3400 Earth radii ( $R_E$ ) for  $V_{\text{SW}} = 500 \text{ km s}^{-1}$ . At the boundary of the MC, the axial field is assumed to be zero. Therefore the constant  $a$  is set to  $J_0^0 / R_{\max}$  where  $J_0^0 \simeq 2.4048$  is the first zero of the  $J_0$  function. The MC model described above allows to consider different orientations of the MC axis, as well as different positions of its axis relative to Earth.

As in this study we focus on how the magnetic structure of MCs changes through the bow shock and during their propagation into the magnetosheath, the density and speed are kept constant throughout the modelled events, whereas the magnetic field strength and direction are allowed to vary. The solar wind is assumed to propagate along the  $x$  direction only, and  $V_{\text{SW}}$  reduces to  $V_x$ . Just downstream of the bow shock, the density, speed and magnetic field magnitude are calculated from the upstream solar wind parameters using the Rankine–Hugoniot relations.

## 3 Validation of the model

### 3.1 Comparison with the Soucek and Escoubet (2012) flow model

In order to check the magnetosheath speed calculation in our model, we compare the obtained velocity profile with the results of Soucek and Escoubet (2012) in the case of a steady solar wind, that is without an MC structure. The upper panel of Fig. 2 shows the magnitude of the flow velocity calculated

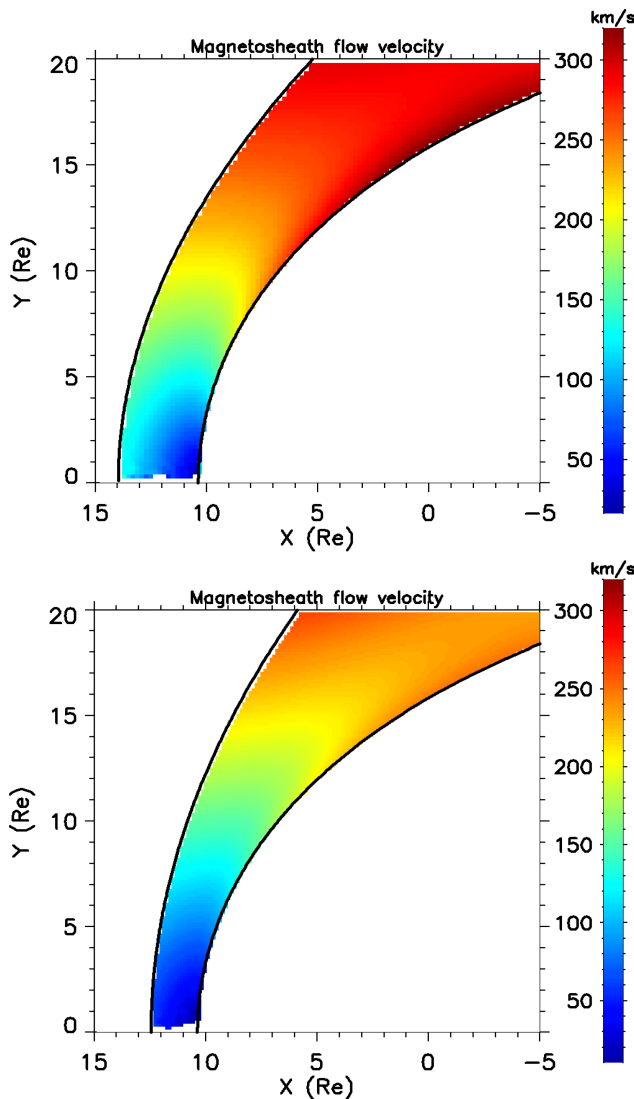


**Fig. 2.** Colour maps of the magnetosheath velocity ( $\text{km s}^{-1}$ ) calculated using the Soucek and Escoubet (2012) model – upper panel: Farris et al. (1991) bow shock model – lower panel: Jeřáb et al. (2005) bow shock model.

in our model with the same upstream solar wind parameters as in Fig. 4 in the paper from Soucek and Escoubet (2012), that is, the parameters from the 6 January 2001 at 00:00 UT ( $V_{\text{SW}} = 410 \text{ km s}^{-1}$ ,  $n_{\text{SW}} = 4.5 \text{ cm}^{-3}$  and  $B = 7.2 \text{ nT}$ ). Note that in the upper panel of Fig. 2, we have used the Farris et al. (1991) bow shock model, as in Soucek and Escoubet (2012). The speed contour lines in Fig. 2 are very similar to those presented by Soucek and Escoubet (2012) in the Fig. 4 of their paper. Analogous velocity contours are also obtained by Génot et al. (2011), when using the Kobel and Flückiger (1994) model as a flow model. Moreover, these results are in qualitative agreement with the MHD simulations performed by Spreiter and Stahara (1994). As expected, the speed is lower everywhere in the dayside magnetosheath than in the

solar wind. Its minimum is reached near the magnetopause subsolar point and the flow velocity increases as it moves tailward.

As explained in Sect. 2.1, in the case of MCs, we use the Jeřáb et al. (2005) bow shock model instead of the Farris et al. (1991) model. The result with the same upstream conditions as above is shown in the lower panel of Fig. 2, but using the Jeřáb et al. (2005) bow shock. The speed magnitude displays the same features as in the upper panel of Fig. 2. Its values change slightly because they depend directly on the solar wind speed tangential component at the bow shock. The Jeřáb et al. (2005) model has a larger flaring than the Farris et al. (1991) model, hence a smaller tangential speed. With the exception of this difference, the results remain consistent with those previously obtained.

### 3.2 Comparison with the Kobel and Flückiger (1994) magnetosheath model

Figure 3 shows the  $B_x$  (first column) and  $B_z$  (second column) components of the magnetosheath magnetic field in the XZ plane. The inputs parameters are a purely southward IMF, where  $B_z = -10 \text{ nT}$ , and regular solar wind plasma parameters,  $V_{\text{SW}} = 400 \text{ km s}^{-1}$  and  $n_{\text{SW}} = 5 \text{ cm}^{-3}$ . The Alfvén Mach number associated with these solar wind conditions is 4.1, which falls into the range of parameters for which the predictive capabilities of the Jeřáb et al. (2005) model have been tested by Turc et al. (2013). The bow shock and magnetopause are described by paraboloids (red and blue dashed lines in Fig. 1).

The upper panels of Fig. 3 correspond to the steady-state magnetosheath magnetic field from the Kobel and Flückiger (1994) model, assuming that the magnetosheath is a current-free region. The  $B_x$  component (Fig. 3a) is positive in the northern part of the magnetosheath and negative in the southern part because of the draping of the field lines around the magnetopause. The increase of the magnetic field strength is highest along the magnetopause, and especially in the subsolar region where the field lines pile up, as it can be seen on the  $B_z$  component (Fig. 3b).

The Fig. 3c and d display our results with the same boundaries as in the Kobel and Flückiger (1994) model, but the magnetic field is propagated step by step along the flowlines, using ideal MHD equations. We find that the magnetic field components calculated by these two models are very similar. The enhancement of the magnetic field strength close to the magnetopause is higher in our MHD calculation than in the Kobel and Flückiger (1994) analytical model, due to the different approach we chose.

The  $B_y$  component (not shown) does not display any particular feature in the XZ plane. The  $B_y$  is equal to zero in the solar wind and remains very small in the magnetosheath in both models. In the equatorial plane (not shown), both magnetic field calculations yield once again very similar results. If we assume a purely northward instead of a purely



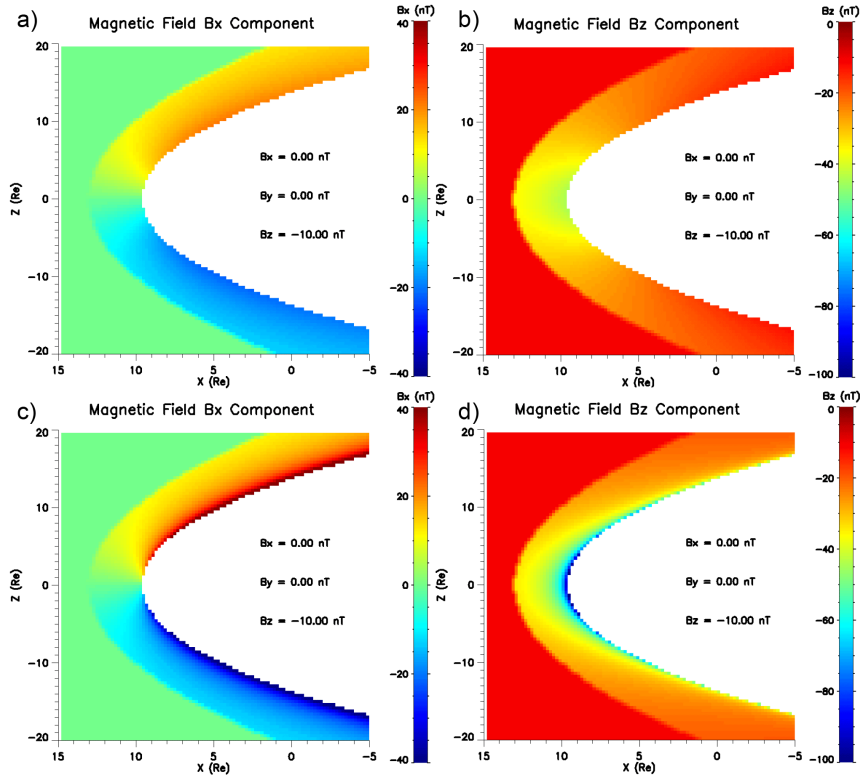


**Fig. 3.** Colour maps of the magnetosheath magnetic field (nT) – left panels:  $B_x$  – right panels:  $B_z$  – upper panels: Kobel and Flückiger (1994) analytic magnetic field model – lower panels: magnetic field propagated with MHD equations along the flowlines. The boundaries of the magnetosheath are calculated with the Kobel and Flückiger (1994) model. The  $B_x$ ,  $B_y$  and  $B_z$  indicated in each plot correspond to the upstream magnetic field components.

southward magnetic field, the only differences observed in the magnetosheath magnetic field are in the signs of  $B_x$  and  $B_z$  which are opposite to what is shown in Fig. 3.

This comparison with the Kobel and Flückiger (1994) model validates our magnetic field propagation method, since no significant difference arises between the two approaches. In the following, the magnetic field will be calculated with our propagation method, which does not require the curl-free assumption and allows time-varying magnetic fields in the solar wind.

## 4 Results

In the following, we will display and discuss the results from our model, first in the case of a steady solar wind with an  $M_A$  comparable to its value during MCs, and then in the case of MCs (i.e. with a slowly rotating magnetic field).

### 4.1 Steady solar wind with purely southward/northward magnetic field

The steady solar wind input parameters are the same as in the previous section, namely,  $B_z = -10$  nT,  $V_{SW} = 400$  km s<sup>-1</sup>

$n_{SW} = 5$  cm<sup>-3</sup> and  $M_A = 4.1$ . Figure 4 shows the outputs of our magnetosheath model in the XZ plane. Note that the colour code changes in each panel and it is indicated in the associated colour bar. Figure 4a and c, corresponding to the  $B_x$  and  $B_z$  components of the magnetic field, respectively, can directly be compared to the results in the Kobel and Flückiger (1994) magnetosheath in Fig. 3. They display very similar features as the other two models presented in Sect. 3.2, even though different models have been used to calculate the magnetosheath shape. The overall structure of the magnetosheath magnetic field, namely, the draping of the field lines, evidenced by the  $B_x$  component (Fig. 4a), and the magnetic field pile-up at the magnetopause on the  $B_z$  (Fig. 4c), remains consistent with what was previously obtained.

No significant feature is observed on the  $B_y$  component (Fig. 4b) which remains very weak, since it is equal to zero in the solar wind and corresponds to the direction perpendicular to the plane of the flow presented here. Therefore it is virtually not modified in the magnetosheath. The slight anti-symmetry between the Northern and Southern hemispheres is most likely caused by the small  $y$  component in

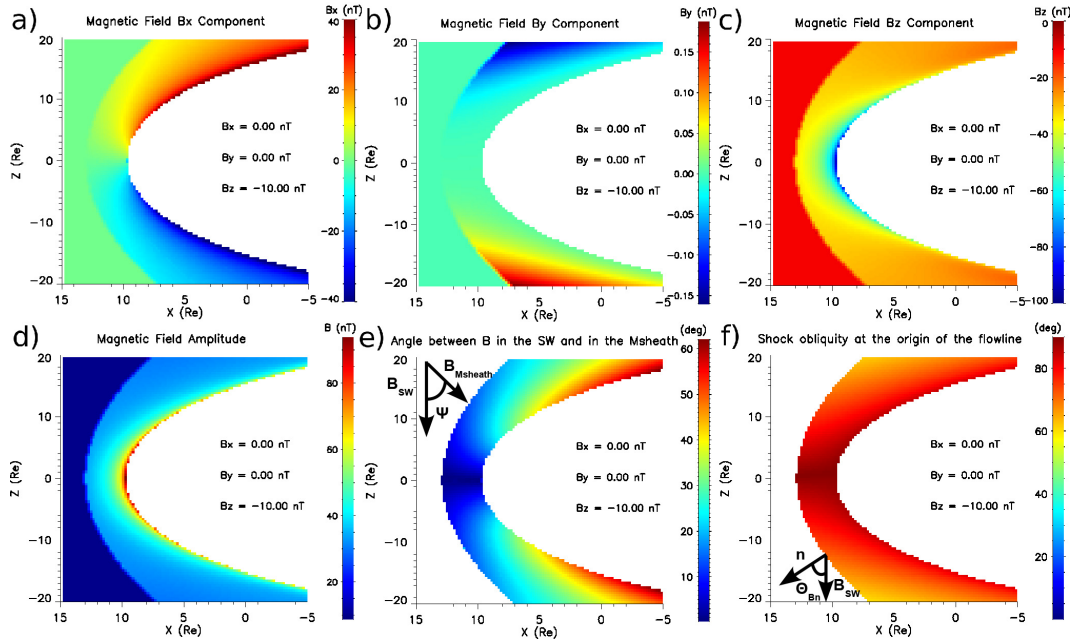


**Fig. 4.** Results of the model for steady solar wind conditions ( $B_z = -10$  nT,  $V_{SW} = 400$  km s $^{-1}$ ,  $n_{SW} = 5$  cm $^{-3}$  and  $M_A = 4.1$ ). The panels correspond to (a)  $B_x$ , (b)  $B_y$ , (c)  $B_z$ , (d)  $B$ , (e)  $\psi$ , the angle between the magnetic field direction in the solar wind and in the magnetosheath, and (f)  $\Theta_{Bn}$ , the shock obliquity at the origin of the flowline.

the normal direction to the bow shock surface, due to its non-axisymmetric shape.

Figure 4d displays the magnetic field magnitude, which is enhanced by a factor of close to 3 at the bow shock's crossing, as expected (Tatallay et al., 1984). Deeper in the magnetosheath, the magnetic field strength increases because of the piling-up of the field lines at the magnetopause. This effect is particularly important in the subsolar region.

In order to illustrate how the magnetic field direction varies across the bow shock, we compute the angle  $\psi$  between the magnetic fields in the magnetosheath and in the solar wind. The values of this angle are presented in the Fig. 4e. At the bow shock's crossing and in the entire subsolar region,  $\psi$  is very small (never exceed  $20^\circ$ ). In particular, in the subsolar region, the magnetic field remains virtually unchanged because the selected IMF is along the  $z$  direction and its direction is not altered by the bow shock's crossing. Since the magnetic field is already tangential to the magnetopause in this region, the draping effects do not alter its direction. When moving tailward, the draping effects come into play and  $\psi$  can reach much higher values along the magnetopause, up to  $70^\circ$ .

One of the key parameters of the bow shock is its obliquity angle, noted as  $\Theta_{Bn}$ , which is defined as the angle between the local normal to the shock's surface and the magnetic field direction in the solar wind. Basically, two different regimes can be defined: the quasi-perpendicular shock, when  $\Theta_{Bn}$  ranges between  $45^\circ$  and  $90^\circ$ , and the quasi-parallel shock, when  $\Theta_{Bn}$  is below  $45^\circ$ . The  $\Theta_{Bn}$  values displayed

in the Fig. 4f are determined at the origin of the flowline of each magnetosheath grid points, in order to relate the magnetosheath parameters to the conditions encountered at the shock. We observe that the entire dayside magnetosheath is located downstream of a quasi-perpendicular bow shock, since the  $\Theta_{Bn}$  values range between  $60^\circ$  and  $90^\circ$ . This is consistent with the absence of significant variation of the magnetic field direction just downstream of the shock (see Fig. 4e) because the magnetic field is mostly tangential to the bow shock's surface and its tangential component is increased by the compression ratio at the bow shock's crossing.

Finally, it should be noted that in the case of a purely southward magnetic field in the solar wind, the magnetosheath displays very symmetric (Fig. 4c to f) or antisymmetric (Fig. 4a and b) features. Similar symmetries and antisymmetries are also observed in the equatorial plane, perpendicular to the plane presented here.

In the case of a purely northward magnetic field, identical results are obtained. The only differences are the sign of the  $B_z$  component, which is negative in the entire magnetosheath, and the sign of  $B_x$  which is opposite to the  $B_x$  shown in Fig. 4a.

## 4.2 Reference MC orientations

We now study how the MCs' structure changes when the MCs cross the bow shock and propagate into the magnetosheath. The MC magnetic field is described by a flux rope model, as detailed in Sect. 2.4. We investigate first the cases



where the MC's axis is parallel to the  $z$  direction and to the  $y$  direction. The values of the solar wind plasma parameters are taken as  $V_{\text{SW}} = 500 \text{ km s}^{-1}$  and  $n_{\text{SW}} = 8.6 \text{ cm}^{-3}$  which roughly correspond to their average value during MCs (Echer et al., 2005; Wu and Lepping, 2011).

MCs can be classified into different categories, depending on the orientation of the flux rope. Many classifications can be found in the literature, generally based on the sign of  $B_z$  in the MC because of its importance for the reconnection processes (see, for example, Bothmer and Schwenn, 1998; Mulligan et al., 1998; Gopalswamy et al., 2008). We will use here the classification introduced by Gopalswamy et al. (2008). According to Gopalswamy et al. (2008), the MCs can be divided into four groups: fully north and fully south, depending on the sign of the axial magnetic field for an axis along  $z$ , and north–south and south–north, corresponding to the  $B_z$  sign in the leading and trailing parts of a flux rope with its axis along  $y$ .

The interaction of an MC propagating along the  $x$  axis towards Earth is schematised in Fig. 5 as seen from above the ecliptic plane. The concentric black circles represent the cross section of an MC modelled by a flux rope. As an example, the axis of this flux rope is perpendicular to the ecliptic plane (i.e. along the  $z$  direction). The  $y_0$  parameter (impact parameter) corresponds to the distance between the intersection of the MC axis with the ecliptic plane and the Sun–Earth line.  $y_0$  is kept constant during the MC's propagation. In a first stage, we will consider central crossings, that is, when  $y_0 = 0$ .

Virtual spacecraft will be used to illustrate the time variation of the magnetic field inside the magnetosheath. They are located in the subsolar region and on the dawn and dusk flanks of the magnetosheath, as indicated by the coloured crosses in Fig. 5, and in the north and dawn flanks (not shown). The virtual spacecraft on the flanks are placed in the dayside magnetosheath so that the draping effects will not be predominant at their location (see the panel e of Fig. 4). Their positions correspond approximately to the regions of the magnetosheath where the Cluster or Themis missions can be found.

Figure 6 shows the temporal variation of the magnetic field during the MC with its axis parallel to the  $z$  direction and with its axial magnetic field pointing to the south. At  $t = 0$ , the MC axis is located at  $x = 3400 R_E$  and  $y_0 = 0$ . It moves at  $V_{\text{SW}} = 500 \text{ km s}^{-1}$  and reaches  $x = -3400 R_E$  at the end of the modelled event. The black lines in Fig. 6 correspond to the solar wind input parameters. In the solar wind, the magnetic field magnitude (Fig. 6a) increases from 10 nT at the beginning of the cloud to 20 nT at its centre, then decreases in the second half of the event. The solar wind  $B_x$  (Fig. 6b) is equal to zero during the entire MC, while the  $B_y$  component (Fig. 6c) changes from positive to negative. The  $B_z$  component (Fig. 6d) is always negative and peaks as  $B_y$  reverses. This MC corresponds to a fully south configuration.

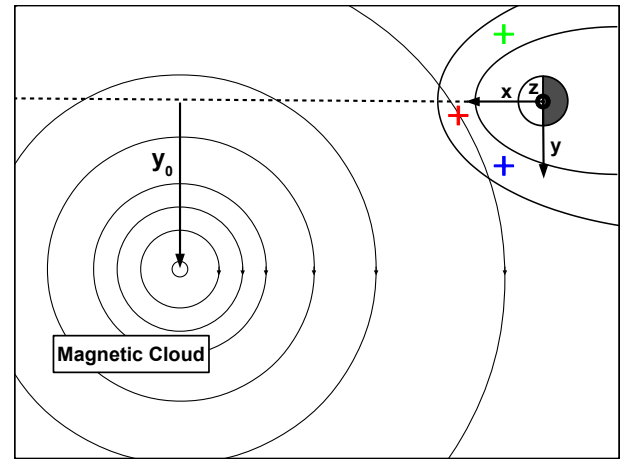


**Fig. 5.** Schematic of an MC's interaction with Earth's environment in our model in the ecliptic plane. The  $y_0$  parameter corresponds to the distance between the intersection of the MC's axis and the Sun–Earth line. The coloured crosses display the approximate location of the virtual spacecraft.

The red, green and blue curves correspond to the measurements from virtual spacecraft in the equatorial magnetosheath, in the subsolar region (red), the dawn flank (green) and the dusk flank (blue) of the magnetosheath, respectively. It is seen that the three virtual spacecraft display quite similar features, although the encountered magnitudes differ. As in the solar wind, the magnetic field strength peaks in the core of the MC (Fig. 6a). The magnetic field magnitude is higher close to the subsolar point (red curve) than farther on the flanks (blue and green curves), most likely because of the piling-up of the field lines in the subsolar region.

Although the  $B_x$  component is equal to zero in the solar wind (Fig. 6b), the bow shock crossing and the draping around the magnetopause distort the field lines and give rise to a  $B_x$  component inside the magnetosheath. The sign of  $B_x$  differs from one side of the magnetosheath (blue and red curves, on the duskside) to another (green curve, on the dawnside) and depends on the sign of the  $B_y$  component in the solar wind because of the flow around the magnetosphere and the orientation of the field lines. The  $B_y$  and  $B_z$  components exhibit similar variations as in the solar wind (Fig. 6c and d).

Figure 6e displays the  $\Theta_{\text{Bn}}$  values calculated at the origin of the flowline on which the spacecraft are located. All three spacecraft remain downstream of a quasi-perpendicular shock during the entire MC. The  $\psi$  angle (Fig. 6f) shows that there is no significant variation of the magnetic field direction from the solar wind to the spacecraft locations ( $\psi \leq 25^\circ$ ). In particular, in the subsolar region (red curve), the values of  $\psi$  remain below  $5^\circ$  during the entire MC. The magnetic structure of the MC is virtually unchanged in this region.

Similar results are obtained if we place two virtual spacecraft in the northern and southern flanks of the magnetosheath (not shown), i.e. perpendicular to the plane

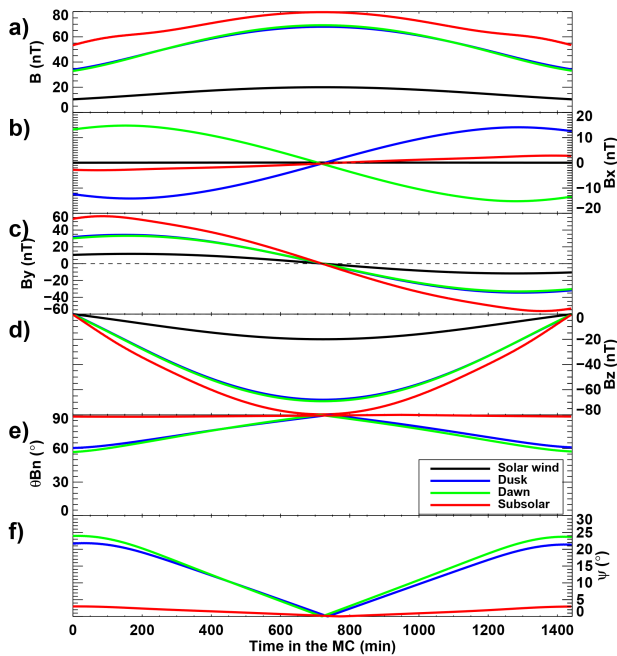


**Fig. 6.** Virtual spacecraft observations of the magnetosheath magnetic field during an MC with its axis along  $z$ . Solar wind inputs (black) – spacecraft: in the subsolar magnetosheath (red), on the dusk flank (blue), on the dawn flank (green) – from top to bottom: magnetic field magnitude,  $B_x$ ,  $B_y$  and  $B_z$  components,  $\Theta_{Bn}$  values at the origin of the flowline and  $\psi$  angle between the magnetic field vectors in the solar wind and in the magnetosheath.

presented previously. If the MC's axis is oriented northward (fully north) instead of southward (not shown), the results are identical, with the exception of the signs of  $B_x$  and  $B_z$  which reverse. If the MC's axis lies along the  $y$  direction (north–south or south–north type MCs, results not shown), the  $B_y$  and  $B_z$  components display an inverted behaviour, compared to the fully south or fully north cases, but the  $B_x$ ,  $\Theta_{Bn}$  and  $\psi$  values remain very similar. Again, we note that the three virtual spacecraft in the magnetosheath observe rather similar temporal magnetic field variations as in the solar wind and are located downstream of a quasi-perpendicular shock. Observations in the XZ plane (not shown) yield similar conclusions for the north–south and south–north type MCs.

In conclusion, no major discrepancy between the virtual spacecraft observations nor between the magnetosheath and the solar wind arises for the centrally encountered MCs with their axis parallel either to the  $z$  or  $y$  direction. The only differences are due to the expected compression and draping of the field lines, but the magnetic field direction is roughly similar almost everywhere in the dayside magnetosheath and in the solar wind, as illustrated by the  $\psi$  values which remain below  $30^\circ$ . In these cases, the magnetosheath is downstream of a quasi-perpendicular bow shock. In these modelled events, the MC's magnetic structure as observed by the

virtual spacecraft does not significantly change from the solar wind to the magnetosheath.

### 4.3 Other configurations

#### 4.3.1 Far-off crossing of a fully south magnetic cloud

Let us now consider the case of a fully south MC, as in Sect. 4.2, but this time encountered very far from its central axis (see Fig. 5). More precisely, its axis is located at  $y_0 = 3000 R_E$  (the chosen radius of the cloud is  $3400 R_E$ ). The core of the MC passes the Earth very far on the duskside and only the MC's edge will interact with the terrestrial magnetosphere. In the cases studied in Sect. 4.2,  $B_x$  was equal to zero. In contrast, the MC magnetic field now presents a large  $B_x$  component, which roughly corresponds to the tangential component  $B_t$  in the frame of the MC (see Eq. 7).

The temporal variations of the magnetosheath magnetic field observed by the virtual spacecraft located in the XY (panel a) and XZ plane (panel b) during this event are displayed in Fig. 7. At  $t = 0$ , the MC's axis is located at  $x = 1660 R_E$ . The three spacecraft in the XZ plane probe the subsolar magnetosheath (purple curves) and the northern (light blue curves) and southern (spring green curves) flanks.

Contrary to what was observed in Sect. 4.2, the magnetosheath magnetic field, as well as its variations, differ now significantly from one spacecraft to another, and from the input parameters. Differences are particularly noticeable on the magnetic field strength (Fig. 7a and g). This parameter previously peaked at the centre of the MC both in the magnetosheath and in the solar wind. Figure 7a and g show that the magnetic field magnitude now has a more complex variation in this MC configuration. For example, the spacecraft on the duskside of the equatorial plane (dark blue line in panel a) encounters its highest magnetic field magnitude at the beginning of the MC, which then steadily decreases until the end of the event. This decrease of the magnetic field strength can be related to the  $\Theta_{Bn}$  values, which diminish concurrently upstream of the same spacecraft from  $60^\circ$  to  $0^\circ$ , because the normal component of the magnetic field becomes predominant and is not modified at the bow shock's crossing. Similar correlations between the variation of the magnetic field magnitude and  $\Theta_{Bn}$  are also observed by the other virtual spacecraft, either in the XY plane or in the XZ plane. We also note that the dawn and dusk spacecraft, as well as the north and south spacecraft, no longer observe the same magnetic field components, in absolute value (see Fig. 7b, c, h and j).

As indicated by the black curves, the magnetic field remains continuously southward in the solar wind during the MC. However, the spacecraft located in the northern magnetosheath encounters a northward  $B_z$  during the entire MC (light blue curve in Fig. 7b). Moreover, even the spacecraft located close to the subsolar region (purple curves) observes a slightly northward  $B_z$  at the beginning and the end of the MC.

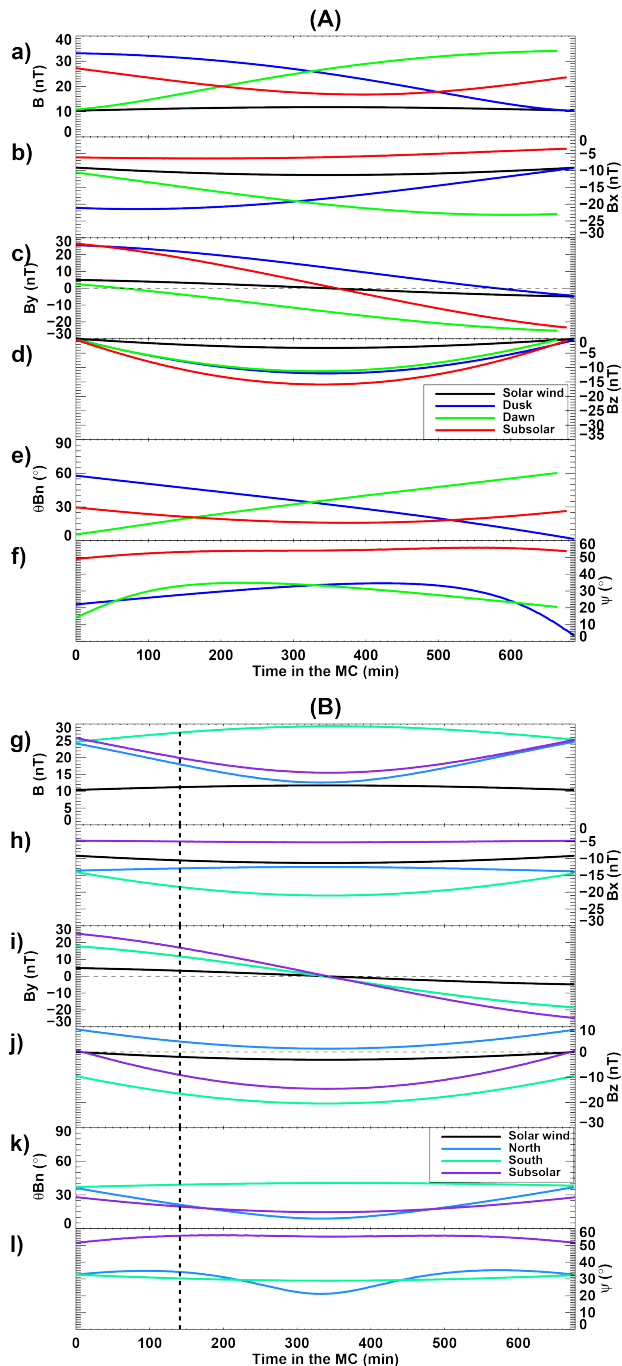


**Fig. 7.** Virtual spacecraft observations of the magnetosheath magnetic field during an MC encountered far from its central axis, in the XY plane (A) and in the XZ plane (B) – spacecraft in (A) see the caption of Fig. 6 – spacecraft in (B) in the subsolar magnetosheath (purple), on the northern flank (light blue), on the southern flank (spring green).

It is also interesting to note that in the leading and the rear parts of the MC, even though the upstream  $B_z$  is close to zero, and negligible compared to the  $B_x$  and  $B_y$ , its relative

importance increases inside the magnetosheath. Indeed, the  $B_z$  values in the northern magnetosheath are around 10 nT, which is comparable to the magnitude of the  $B_x$  and  $B_y$  components, around 15 and 20 nT, respectively. A negligible  $B_z$  in the solar wind can become, if not predominant, at least significant in the magnetosheath.

For MCs shown in Sect. 4.2, the shock configuration remains quasi-perpendicular. On the contrary, the  $\Theta_{Bn}$  values in Fig. 7e and k indicate that all the virtual spacecraft are located downstream of a quasi-parallel shock, at least during a part of the modelled event. Moreover, the variations of the  $\Theta_{Bn}$  values are much larger here than in the previous cases. In some parts of the magnetosheath, the shock configuration turns from quasi-perpendicular to quasi-parallel, or conversely (see the green and blue curves in Fig. 7e), as the MC passes by Earth's environment.

The MC's structure in the subsolar region differs now strikingly from that in the solar wind: very large variations of the magnetic field direction are observed in the subsolar region, as evidenced by the  $\psi$  values around 60° (Fig. 7f and l, red and purple curves). In the other four locations, the  $\psi$  values remain roughly around 30°. These values are comparable to that encountered during the reference MCs in Sect. 4.2. However, it should be noted that in the previous cases, the  $\psi$  values did not exceed 20° for more than half of the MC duration. Therefore, the changes in the MC's structure are more significant in the present case.

We note that the green, dark blue (in panel a) and light blue (in panel b) virtual spacecraft observe a decrease in  $\psi$  associated with very low  $\Theta_{Bn}$  values ( $\Theta_{Bn} \lesssim 15^\circ$ ). In the strictly parallel limit, the magnetic field direction is expected not to be altered by the bow shock crossing, as its normal component traverses unchanged. This may explain the decrease of the  $\psi$  values observed by these three virtual spacecraft.

As an example, a snapshot of the magnetosheath in the XZ plane is given in Fig. 8. It corresponds to the magnetosheath state when the MC's axis is at  $x = 1000 R_E$  upstream of Earth's environment (i.e. about 140 min after the edge of the MC reached the bow shock). The time of the snapshot is indicated by a vertical dashed line in Fig. 7.

The major difference between the case presented here and the examples detailed in Sect. 4.2 is the shock configuration which is quasi-parallel instead of quasi-perpendicular.  $\Theta_{Bn}$  ranges between 15° and 45° in the XZ plane (Fig. 8f), and is mostly below 20° in the northern magnetosheath. These low  $\Theta_{Bn}$  values are accompanied by a large variation of the magnetic field direction at the bow shock's crossing, as it can be seen on the angle  $\psi$  in Fig. 8e. Just downstream of the shock,  $\psi$  ranges between 20° and 40°, whereas its variation did not exceed 20° at the shock in the previous examples (not shown). Therefore, the magnetic field direction is already strongly modified just downstream of the bow shock. Deeper in the magnetosheath,  $\psi$  increases, up to 65°, because of the draping effects. Moreover, the magnetosheath magnetic field now displays very strong asymmetries. For example, the  $B_x$

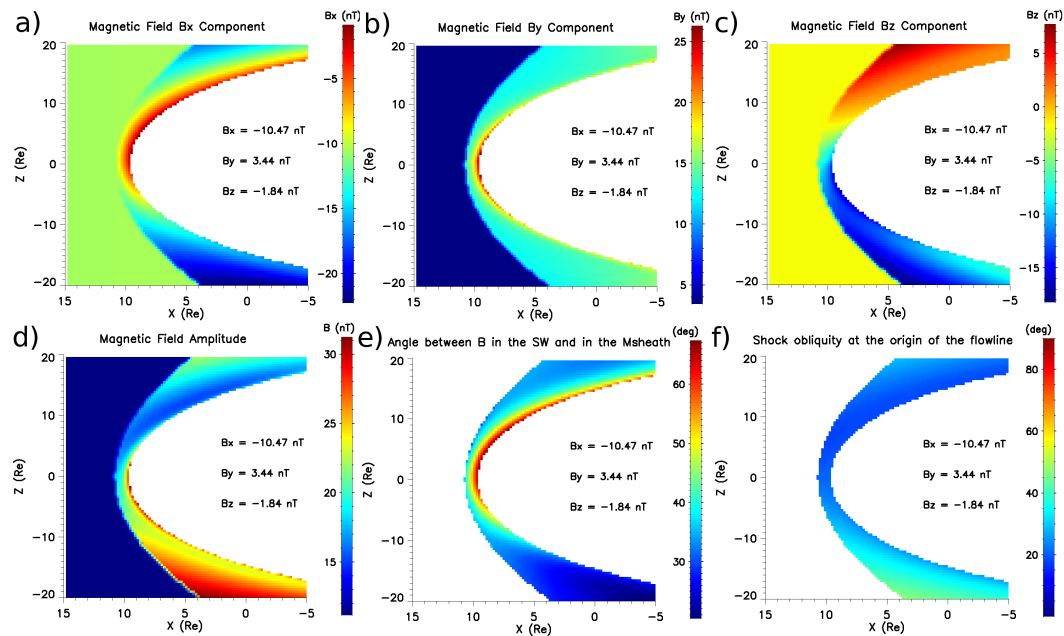


**Fig. 8.** Snapshots of the magnetosheath during an MC with its axis along  $z$ , encountered far from its centre, when the axis is located at  $x = 1000 R_E$ . The panels correspond to (a)  $B_x$ , (b)  $B_y$ , (c)  $B_z$ , (d)  $B$ , (e)  $\psi$ , the angle between the magnetic field direction in the solar wind and in the magnetosheath, and (f)  $\Theta_{Bn}$ , the shock obliquity at the origin of the flowline.

component observed along the northern magnetopause (upper part of Fig. 8a) is around zero, whereas its values along the southern magnetopause are below  $-20$  nT.

More importantly, large asymmetries also arise in the magnetic field strength. Instead of a situation where the magnetic field strength increases when moving closer to the magnetopause, as in Fig. 4d, Fig. 8d evidences a much more complicated structure. Whereas some parts of the magnetosheath still display an enhancement of the magnetic field magnitude close to the magnetopause, for example in the Southern Hemisphere (lower part of Fig. 8d), low magnetic field values are observed even close to the northern magnetopause (upper part of Fig. 8d). The very small magnetic field strength is presumably due to the weak compression downstream of the quasi-parallel shock (see Fig. 8f). These large variations of the magnetic field strength imply that the magnetic pressure impacting the magnetopause will strongly depend on the location. This may result in asymmetric shapes of the magnetopause and magnetosheath, not taken into account here, and possibly in asymmetric current circulation in the magnetosheath.

One of the most interesting features of this example is the reversal of the  $B_z$  component in a large part of the northern magnetosheath (Fig. 8c). In order to illustrate the extent of this phenomenon, a map of the magnetosheath magnetic field near the magnetopause is displayed in Fig. 9. In this polar map, the distance from the centre corresponds to the zenithal angle (i.e. the angle from the Sun–Earth line) between 0 and  $90^\circ$ . The azimuthal direction corresponds to the

clock angle, defined as the direction in the plane perpendicular to the Sun–Earth line. The subsolar point is indicated by the black cross at the centre of the map. The map in Fig. 9 has been determined at the same time during the MC as the snapshots in Fig. 8.

Figure 9 shows that the  $B_z$  component is positive in a large part of the dawnside of the northern magnetosheath. According to this map, approximately one quarter of the dayside magnetopause actually encounters a northward  $B_z$  while the solar wind  $B_z$  is negative. Moreover, the location and the extent of the reversed  $B_z$  region vary as the MC passes by Earth's environment (not shown). Similarly, if we consider the same MC, but with a northward axial field, the positive  $B_z$  upstream of the shock will also reverse. The dawnside of the southern magnetosheath will encounter a negative  $B_z$ .

#### 4.3.2 Central crossing of a largely tilted magnetic cloud

The last example that we will consider here is the central crossing ( $y_0 = 0$ ) of an MC with its axis largely tilted with respect to the YZ plane (the axes of the previous example MCs all lied in the YZ plane). More precisely, the axis direction is  $\theta_{MC} = 70^\circ$  and  $\phi_{MC} = 20^\circ$ , where  $\theta_{MC}$  is the colatitude and  $\phi_{MC}$  the longitude. The virtual spacecraft observations in the XZ plane during this event are displayed in Fig. 10. As in the example shown in Sect. 4.3.1, the upstream MC magnetic field has a large  $B_x$  component ( $\simeq 10$  nT).

Again, the magnetic field direction strongly differs from one spacecraft to another and compared to the input



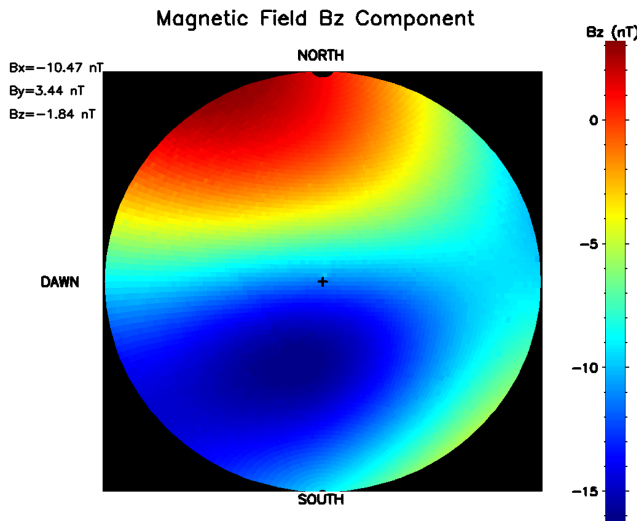


**Fig. 9.** Colour map of the  $B_z$  component in the magnetosheath along the magnetopause during a fully south MC, encountered far from its centre, when the axis is located at  $x = 1000 R_E$ . The centre of the plot corresponds to the subsolar point. The radial distance from the subsolar point is proportional to the zenithal angle. The magnetic field components indicated on the upper left of the map are the solar wind magnetic field inputs.

parameters, as shown by the magnetic field components and the angle  $\psi$ . It is interesting to note that the spacecraft in the southern magnetosheath (spring green curves) encounters a magnetic structure rather similar to that in the solar wind ( $\psi \leq 30^\circ$ ), while the two other spacecraft observe concurrently completely different magnetic field orientations ( $\psi \geq 30^\circ$ ) (Fig. 10f). The structure of the MC varies greatly depending on the considered region, and particularly in the subsolar region (purple curve) where  $\psi$  reaches values as high as  $60^\circ$ . The  $\Theta_{Bn}$  values (Fig. 10e) are rather low, corresponding to a quasi-parallel (blue and purple curves) or oblique (spring green curves) shock configuration.

The upstream values of the  $B_z$  show that this component turns south in the last hours of the MC (Fig. 10d). In the magnetosheath, however, the sign of  $B_z$  changes at different times, the earliest being for the spacecraft in the northern magnetosheath (blue curve), or even does not reverse, as observed by the spacecraft in the southern magnetosheath (spring green curve). Depending on the spacecraft we rely on, the duration of the southward  $B_z$  part of the MC differs and different conclusions would be drawn in terms of geoeffectivity.

To conclude, we have shown that in certain MC configurations, their magnetic structure can be modified from the solar wind to the magnetosheath. Moreover, this structure changes from one region of the magnetosheath to another and varies with time as the MC passes by Earth's environment. In both cases presented here, the shock configuration remains quasi-parallel during most of the MC, and even just downstream of

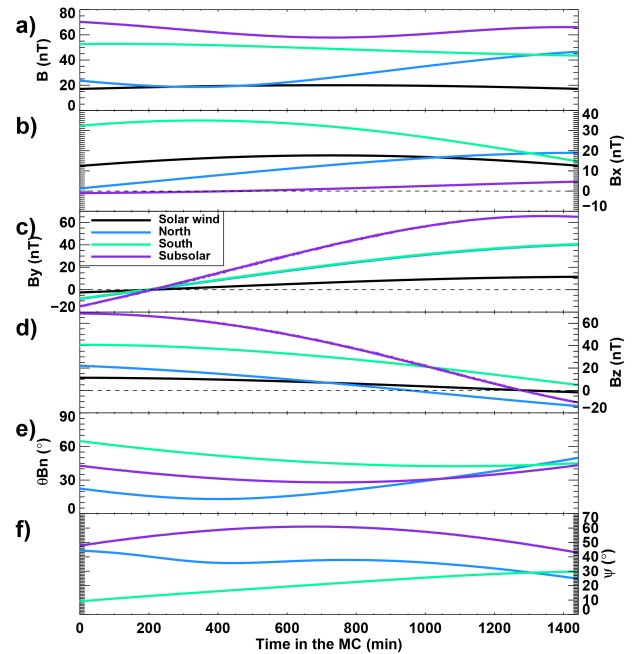


**Fig. 10.** Virtual spacecraft observations of the magnetosheath magnetic field during an oblique MC. See the caption of the panel B of Fig. 7 for details.

the bow shock, the magnetic field direction strongly differs from its upstream orientation.

## 5 Consequences on geoeffectivity

The geoeffectivity of MCs is generally estimated from the sign of the  $B_z$  component during the cloud. This is due to the fact that in the equatorial plane Earth's dipolar magnetic field is essentially northward. Therefore, a southward magnetic field upstream of the magnetopause, that is anti-parallel to Earth's equatorial field, is favourable to reconnection processes (Dungey, 1961). Reconnection is more effective and induces larger disturbances in Earth's magnetosphere when it occurs in the subsolar region (see, for example, the review of Paschmann, 2008). Yet reconnection can occur anywhere along the magnetopause, as soon as there are anti-parallel magnetic fields.

The magnetosheath model presented in this work does not describe reconnection processes. However, it can be used to determine where anti-parallel magnetic fields can be found at the magnetopause, by providing the magnetosheath magnetic field near this boundary. An example of a map of the  $B_z$  component of the magnetosheath magnetic field near the magnetopause is given in Fig. 9. Similarly, we can have access to all three components for any MC configuration. We calculate the magnetospheric magnetic field using the T96 model (Tsyganenko, 1995, 1996), available at <http://geo.phys.spbu.ru/~tsyganenko/modeling.html>. Earth's

internal magnetic field is assumed to be a dipole. Since our magnetosheath model is rather crude, using the International Geomagnetic Reference Field instead of a dipole to model more accurately the geomagnetic field would not bring further information suitable for this study. The T96 model takes into account the tilt of Earth's dipole. Since we only model here synthetic cases, which do not correspond to real events, we will arbitrarily choose the orientation of the dipole corresponding to the 21 December 2002 at noon. We checked that the results were similar for other dates. The T96 model requires the upstream solar wind speed, dynamic pressure and the  $B_y$  and  $B_z$  component of the magnetic field, as well as the disturbance storm time (Dst) index, as inputs. The Dst index is set to zero and we checked that the location of anti-parallel fields along the magnetopause is not significantly sensitive to the Dst, even with large negative Dst values which are expected to stretch the magnetospheric field. In order to estimate where anti-parallel fields can be found, we compute the shear angle along the magnetopause, i.e. the angle between the magnetosheath and magnetospheric magnetic field vectors just upstream and downstream of the magnetopause.

First, we will examine the case of the centrally crossed fully south MC. As the MC passes by Earth's environment, the magnetic field turns from an eastward orientation to a southward field at the centre of the cloud, and finally to a westward orientation at the rear. The magnetic field orientation in the leading and trailing parts of the MC are not expected to be favourable to reconnection. However, when moving towards the centre of the MC,  $B_z$  turns south and should become increasingly propitious to reconnection processes. Concurrently, the effects of the MC on the magnetosphere should be enhanced. The values of the shear angle along the magnetopause are displayed in Fig. 11 at three different times during the MC, corresponding roughly to these three orientations of the magnetic field, in the same frame as in Fig. 9.

The upper panel corresponds to the beginning of the MC (i.e. when its centre is located at  $x = 3000 R_E$  upstream of Earth). The upstream magnetic field is mainly along  $B_y$ . Anti-parallel fields are primarily found on the dawnside magnetopause, quite close to the subsolar region (red areas in Fig. 11). As the MC travels past the Earth, however, the location of the anti-parallel field region changes. In the core of the MC (middle panel), its position has moved closer to the subsolar point, and a little northward of it due to the dipole tilt. This middle panel is actually rather similar to the usual picture, since the upstream magnetic field is then essentially southward. Finally, at the end of the MC (bottom panel), the anti-parallel field region has rotated duskward.

The point here is that the location and the extent of the anti-parallel magnetic field region change with the orientation of the MC's magnetic field. The efficiency of reconnection processes is maximum at the subsolar point (Paschmann, 2008, and references therein). In the centre of this MC, the anti-parallel fields are found in the vicinity of the subsolar

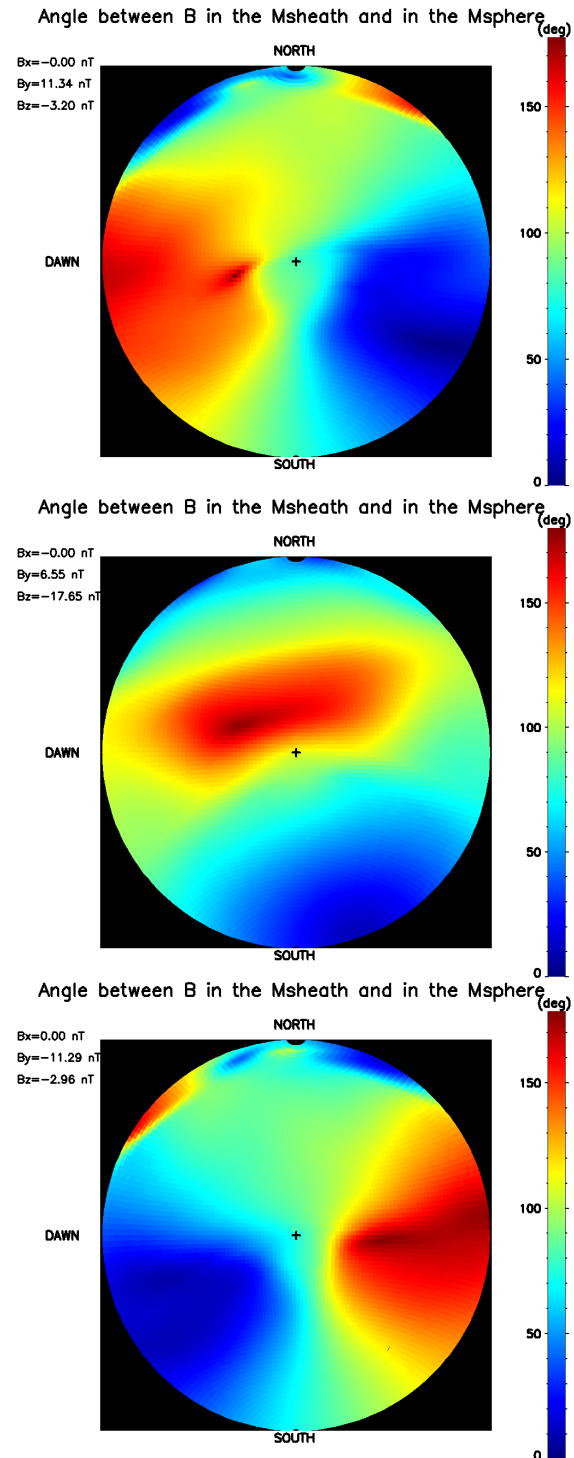


**Fig. 11.** Colour maps of the shear angle along the magnetopause during the central crossing of a fully south MC. See the caption of Fig. 9 for details. Top panel: at the beginning of the MC ( $x = 3000 R_E$ ) – middle panel: in the core of the MC ( $x = 1000 R_E$ ) – bottom panel: at the end of the MC ( $x = -3000 R_E$ ).



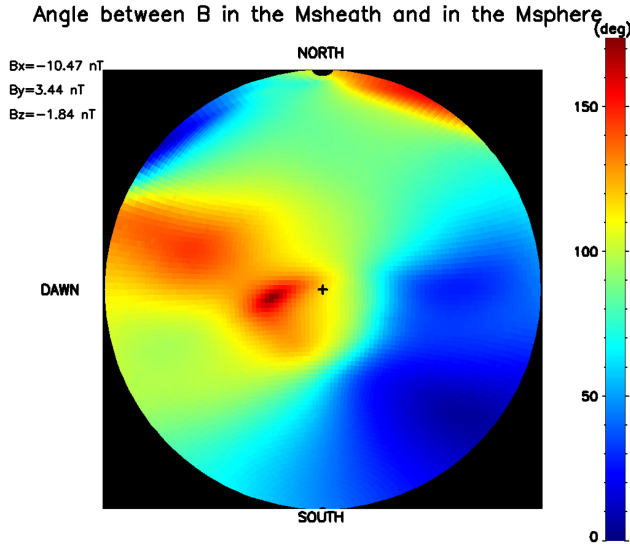


**Fig. 12.** Colour map of the shear angle along the magnetopause during the far-off crossing of a fully south MC when its axis is located at  $x = 1000 R_E$  upstream of Earth. See the caption of Fig. 9 for details.

point. The maximum reconnection rate would probably be observed at this time. Yet reconnection may also occur when the magnetic field turns east or west and may be effective since the anti-parallel field region comes rather close to the subsolar magnetopause. Therefore, geomagnetic disturbances may be observed also during the leading and trailing parts of this MC.

If the axial magnetic field inside the MC points north instead of south, anti-parallel fields are again found on the dawnside and duskside magnetopause, at the beginning and at the end of the cloud, respectively. In the centre of the MC, the magnetosheath magnetic field is essentially along  $+B_z$  and the anti-parallel field regions are observed at high latitudes, corresponding to the expected lobe reconnection for a northward magnetic field.

Similar conclusions are drawn in the case of the north-south MC. The only difference between these two configurations is the order in which these regions of anti-parallel fields arise. We first observe a northward field, during which the reconnection regions are located close to the poles. Then during the eastward and southward parts of the MC, the obtained results are comparable to the upper and middle panels of Fig. 11, respectively. Note that even if  $B_z$  is smaller in the north-south case than in the fully south or fully north cases, where  $B_z$  is the axial field, it does not affect significantly the regions of anti-parallel fields.

In Sect. 4.3.1, we have shown that when a fully south MC is crossed far from its centre, the bow shock is in a quasi-parallel configuration and that  $B_z$  reverses in the northern magnetosheath. The shear angle at the magnetopause for such an MC is displayed in Fig. 12, in the same frame as in

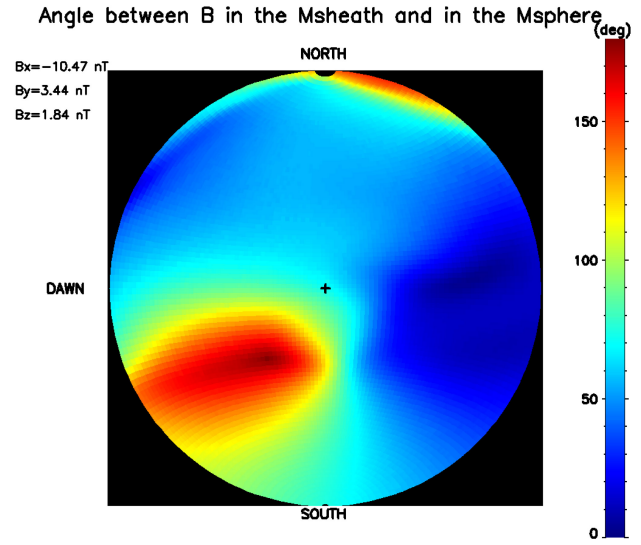


**Fig. 13.** Colour maps of the shear angle along the magnetopause during the far-off crossing of a fully north MC when its axis is located at  $x = 1000 R_E$  upstream of Earth. See the caption of Fig. 9 for details.

Fig. 11. It is calculated in the same conditions as the snapshots of the magnetosheath in Fig. 8 (i.e. when the axis of the MC is at  $x = 1000 R_E$  upstream of Earth). As expected from a southward  $B_z$ , anti-parallel fields are found in the equatorial plane. Similarly to the upper panel of Fig. 11, they mostly lie close to the subsolar region, on the dawnside, with the exception of a small area near the North Pole. In both cases, it is due to the positive  $B_y$  in the MC, which remains positive in the entire dayside magnetosheath, whereas the sign of the magnetospheric  $B_y$  changes from the dawnside to the duskside. When approaching the central part of the MC, the anti-parallel field region moves closer to the subsolar point. It is then observed on the duskside in the rear part of the MC (not shown).

Figure 13 corresponds to the fully north configuration. Thus, the only difference to the map in Fig. 12 is the sign of  $B_z$ , while the other magnetic field components remain identical. According to the sign of the  $B_z$  upstream of the bow shock, reconnection is only expected to take place at high latitudes. However, in the same way as  $B_z$  turns from south to north in the northern magnetosheath in the fully south configuration, the  $B_z$  component of the fully north MC reverses in the dawnside of the southern magnetosheath where it becomes negative (not shown). The shear angle at the magnetopause demonstrates that anti-parallel field lines are indeed found in this region, rather close to the subsolar point (red area in Fig. 13). These may lead to significant reconnection rates. Therefore, even if a northward  $B_z$  is observed in the solar wind, its orientation can change before it reaches the magnetopause and become favourable to reconnection.

It can also be noted that the cases shown in Figs. 12 and 13 both correspond to MCs encountered far from their central axis. It is generally admitted that centrally crossed MCs tend to be more geoeffective because of their higher magnetic field magnitude and the stronger shock ahead of them. Yet the results displayed in Figs. 12 and 13 hint at the significance of far-off encounters, which may also lead to strong geomagnetic activity.

## 6 Discussion and conclusions

In this paper, we have introduced the first magnetosheath model adapted to MCs conditions, and applied it to MCs with different axis orientations and impact parameters. This model describes how the structure of MCs is modified by the bow shock's crossing and during their propagation into the magnetosheath. The magnetosheath flow is calculated with the Soucek and Escoubet (2012) model, which is adapted to fit the Shue et al. (1998) magnetopause and the Jeřáb et al. (2005) bow shock models. The magnetic field is computed along the flowlines from ideal MHD equations. In a first stage, we focus on centrally crossed MCs with their axis along  $z$  or  $y$ . We show that in these cases the dayside bow shock is essentially in a quasi-perpendicular configuration and that the magnetic structure of the MCs is roughly preserved in the dayside magnetosheath ( $\psi \leq 30^\circ$ ). As expected, close to the magnetopause, the draping of the field lines around the magnetosphere tends to alter the MC's structure.

We then investigate other MC configurations, namely, the far-off crossing of a fully south MC and the central crossing of an MC with a large tilt towards the ecliptic plane. In both cases, it appears that the MC's magnetic structure is greatly modified inside the magnetosheath, and that these changes depend on the considered region of the magnetosheath. Just downstream of the bow shock, where the draping effects do not come into play, the magnetic field direction already strongly differs from its upstream orientation. Therefore, the observed differences can be related to the quasi-parallel shock configuration. Besides,  $B_z$  even reverses in some parts of the magnetosheath.

Finally, we use a magnetospheric magnetic field model combined with our magnetosheath magnetic field calculations to estimate the location of the regions of anti-parallel magnetic fields. We show that they vary as the MCs pass by the Earth. Moreover, these regions may arise close to the subsolar magnetopause even during a fully north MC, leading possibly to significant reconnection rates. Although the magnetospheric disturbances induced by fully north MCs are generally attributed to the sheath fields or other southward fields (Zhang et al., 2004; Huttunen et al., 2005), the magnetic fields inside the MC could contribute to the geomagnetic activity. We also stress the fact that an MC crossed far from its central part may also be geoeffective.

The results of this work point out the major role played by the shock configuration in modifying or keeping unchanged the MC's structure. If an MC encounters a quasi-perpendicular shock, its downstream structure will most likely be very similar to that observed in the solar wind, at least in the dayside magnetosheath. In such case, the magnetic field direction impacting the magnetopause can be approximated by the IMF direction. The predictions on the MC's geoeffectivity will not differ much by considering either the solar wind magnetic field or the magnetosheath magnetic field. This scenario is encountered when the MC's axis is perpendicular to the Sun–Earth line. On the contrary, if an MC encounters a quasi-parallel configuration, its structure will be altered by the shock's crossing. The assumption that the magnetic field direction remains unchanged from the solar wind to the magnetopause does no longer hold, as  $\psi$  can reach values as high as  $60^\circ$ . Thus, the MC's geoeffectivity may differ from what was expected from the solar wind observations. This is observed when the MC is encountered far from its central axis or when its axis is largely tilted towards the ecliptic plane.

The complex physics of the quasi-parallel shock cannot be described properly by our simple magnetosheath model based on ideal MHD. Many phenomena due to the quasi-parallel regime, such as turbulence and other microphysics processes, play a major role on the magnetosheath properties downstream of the quasi-parallel bow shock but cannot be included in our model. However, some features obtained with our model are consistent with what is expected downstream of the quasi-parallel shock, in particular the lesser compression as  $\Theta_{Bn}$  decreases. Consequently, in some regions of the magnetosheath, the magnetic pressure is stronger than in others. In the example presented in Sect. 4.3.1, the variations of the magnetic pressure range between 5 % and 16 % of the dynamic pressure at the magnetopause because of the high magnetic field strength in the MC. Therefore, the variations in the magnetic pressure may impact the magnetopause location and shape, as it will be more compressed where the magnetic pressure is higher. This asymmetric compression will probably have consequences in the magnetosphere, particularly on the current systems, but this lies beyond the scope of this paper.

The knowledge of the shock obliquity appears to be crucial to determine the MC's structure inside the magnetosheath. Yet spacecraft observations seldom provide us with this parameter, since it is generally obtained from direct observations of bow shock crossings. In most cases, we have to rely on a model to estimate the  $\Theta_{Bn}$  values, as was done in this work. But even without a bow shock model, the  $B_x$  component of the upstream magnetic field can already give information about the shock configuration. Indeed, the quasi-parallel region moves closer to the subsolar region as the importance of  $B_x$  increases in the solar wind.

Therefore, we can infer that the more predominant the  $B_x$  component is in an MC, the more likely its structure is to

be altered in the magnetosheath. In terms of flux rope orientations, it corresponds to MCs encountered far from their central axis, or with an axis lying close to the ecliptic plane (and outside the YZ plane). In such configurations, large asymmetries in the magnetosheath magnetic field are expected to arise, and the  $B_z$  component may even reverse in some parts of the magnetosheath. This reversal is observed when the upstream  $B_z$  is rather small.

Finally, we can infer that during an MC, if different spacecraft observe the same structure in the solar wind and in the magnetosheath, then the spacecraft in the magnetosheath are probably located downstream of a quasi-perpendicular shock. The MC orientation would possibly correspond to the central crossing of a flux rope whose axis lies close to the YZ plane. In this case, the  $B_x$  component remains very small relative to the others inside the MC, maintaining the quasi-perpendicular shock configuration. On the contrary, if spacecraft located at different places inside the magnetosheath observe different magnetic structures, we can infer that the shock configuration varies largely along the bow shock and that a quasi-parallel regime can presumably be found in some parts of the magnetosheath. As stated earlier, this would correspond to an MC with a substantial  $B_x$  component (i.e. a largely tilted flux rope or a far-off encounter).

The results of the present work can also directly be used to interpret spacecraft observations of MCs in the magnetosheath by complementing a limited data set along their orbit with an overview of the magnetosheath magnetic field. The comparison between spacecraft observations and this model's outputs will be the topic of an upcoming study.

In addition to MC studies, this model can also be used to describe the steady-state magnetosheath for a given IMF orientation, during low  $M_A$  conditions. Moreover, since MCs are large-scale structures, the magnetic field is roughly the same everywhere along the bow shock and its rotation is slow compared to the plasma flow time inside the magnetosheath. Therefore, the snapshots of the magnetosheath, as well as each time step of the time series, given in Sect. 4 and 5, can be interpreted as the magnetosheath state for the corresponding upstream conditions.

To conclude, even though this model is rather crude, it yields a first approach of the interaction between MCs and Earth's bow shock and of their propagation into the magnetosheath. It outlines the importance of taking into account the magnetosheath to estimate an MC's geoeffectivity.

Topical Editor L. Blomberg thanks two anonymous referees for their help in evaluating this paper.

## References

- Bothmer, V. and Schwenn, R.: The structure and origin of magnetic clouds in the solar wind, *Ann. Geophys.*, 16, 1–24, doi:10.1007/s00585-997-0001-x, 1998.
- Burlaga, L., Sittler, E., Mariani, F., and Schwenn, R.: Magnetic loop behind an interplanetary shock – Voyager, Helios, and IMP 8 observations, *J. Geophys. Res.*, 86, 6673–6684, doi:10.1029/JA086iA08p06673, 1981.
- Burlaga, L. F.: Magnetic clouds and force-free fields with constant alpha, *J. Geophys. Res.*, 93, 7217–7224, 1988.
- Chen, J., Slinker, S. P., and Triandaf, I.: Bayesian prediction of geomagnetic storms: Wind data, 1996–2010, *Space Weather*, 10, S04005, doi:10.1029/2011SW000740, 2012.
- Coleman, I. J.: A multi-spacecraft survey of magnetic field line draping in the dayside magnetosheath, *Ann. Geophys.*, 23, 885–900, doi:10.5194/angeo-23-885-2005, 2005.
- Dungey, J. W.: Interplanetary Magnetic Field and the Auroral Zones, *Phys. Rev. Lett.*, 6, 47–48, doi:10.1103/PhysRevLett.6.47, 1961.
- Echer, E., Alves, M. V., and Gonzalez, W. D.: A statistical study of magnetic cloud parameters and geoeffectiveness, *J. Atmos. Sol.-Terr. Phys.*, 67, 839–852, doi:10.1016/j.jastp.2005.02.010, 2005.
- Echer, E., Gonzalez, W. D., Tsurutani, B. T., and Gonzalez, A. L. C.: Interplanetary conditions causing intense geomagnetic storms ( $Dst \leq -100$  nT) during solar cycle 23 (1996–2006), *J. Geophys. Res.*, 113, A05221, doi:10.1029/2007JA012744, 2008.
- Farris, M. H. and Russell, C. T.: Determining the standoff distance of the bow shock: Mach number dependence and use of models, *J. Geophys. Res.*, 99, 17681, doi:10.1029/94JA01020, 1994.
- Farris, M. H., Petriner, S. M., and Russell, C. T.: The thickness of the magnetosheath – Constraints on the polytropic index, *Geophys. Res. Lett.*, 18, 1821–1824, doi:10.1029/91GL02090, 1991.
- Génot, V., Broussillou, L., Budnik, E., Hellinger, P., Trávníček, P. M., Lucek, E., and Dandouras, I.: Timing mirror structures observed by Cluster with a magnetosheath flow model, *Ann. Geophys.*, 29, 1849–1860, doi:10.5194/angeo-29-1849-2011, 2011.
- Gopalswamy, N., Akiyama, S., Yashiro, S., Michalek, G., and Lepping, R. P.: Solar sources and geospace consequences of interplanetary magnetic clouds observed during solar cycle 23, *J. Atmos. Sol.-Terr. Phys.*, 70, 245–253, doi:10.1016/j.jastp.2007.08.070, 2008.
- Huttunen, K. E. J., Schwenn, R., Bothmer, V., and Koskinen, H. E. J.: Properties and geoeffectiveness of magnetic clouds in the rising, maximum and early declining phases of solar cycle 23, *Ann. Geophys.*, 23, 625–641, doi:10.5194/angeo-23-625-2005, 2005.
- Jeřáb, M., Němeček, Z., Šafránková, J., Jelínek, K., and Měrka, J.: Improved bow shock model with dependence on the IMF strength, *Planet. Space Sci.*, 53, 85–93, doi:10.1016/j.pss.2004.09.032, 2005.
- Kallio, E. J. and Koskinen, H. E. J.: A semiempirical magnetosheath model to analyze the solar wind-magnetosphere interaction, *J. Geophys. Res.*, 105, 27469–27480, doi:10.1029/2000JA900086, 2000.
- Kobel, E. and Flückiger, E. O.: A model of the steady state magnetic field in the magnetosheath, *J. Geophys. Res.*, 99, 23617–23622, doi:10.1029/94JA01778, 1994.

- Lavraud, B. and Borovsky, J. E.: Altered solar wind-magnetosphere interaction at low Mach numbers: Coronal mass ejections, *J. Geophys. Res.*, 113, A00B08, doi:10.1029/2008JA013192, 2008.
- Lavraud, B., Larroque, E., Budnik, E., Génot, V., Borovsky, J. E., Dunlop, M. W., Foullon, C., Hasegawa, H., Jacquey, C., Nykyri, K., Ruffenach, A., Taylor, M. G. G. T., Dandouras, I., and Rème, H.: Asymmetry of magnetosheath flows and magnetopause shape during low Alfvén Mach number solar wind, *J. Geophys. Res.*, 118, 1089–1100, doi:10.1002/jgra.50145, 2013.
- Lepping, R. P., Berdichevsky, D. B., Wu, C.-C., Szabo, A., Narock, T., Mariani, F., Lazarus, A. J., and Quivers, A. J.: A summary of WIND magnetic clouds for years 1995–2003: model-fitted parameters, associated errors and classifications, *Ann. Geophys.*, 24, 215–245, doi:10.5194/angeo-24-215-2006, 2006.
- Longmore, M., Schwartz, S. J., Geach, J., Cooling, B. M. A., Dandouras, I., Lucek, E. A., and Fazakerley, A. N.: Dawn-dusk asymmetries and sub-Alfvénic flow in the high and low latitude magnetosheath, *Ann. Geophys.*, 23, 3351–3364, doi:10.5194/angeo-23-3351-2005, 2005.
- Longmore, M., Schwartz, S. J., and Lucek, E. A.: Rotation of the magnetic field in Earth's magnetosheath by bulk magnetosheath plasma flow, *Ann. Geophys.*, 24, 339–354, doi:10.5194/angeo-24-339-2006, 2006.
- Mërka, J., Szabo, A., Narock, T. W., King, J. H., Paularena, K. I., and Richardson, J. D.: A comparison of IMP 8 observed bow shock positions with model predictions, *J. Geophys. Res.*, 108, 1077, doi:10.1029/2002JA009384, 2003.
- Mulligan, T., Russell, C. T., and Luhmann, J. G.: Solar cycle evolution of the structure of magnetic clouds in the inner heliosphere, *Geophys. Res. Lett.*, 25, 2959–2963, doi:10.1029/98GL01302, 1998.
- Paschmann, G.: Recent in-situ observations of magnetic reconnection in near-Earth space, *Geophys. Res. Lett.*, 35, 19109, doi:10.1029/2008GL035297, 2008.
- Richardson, I. G. and Cane, H. V.: Near-Earth Interplanetary Coronal Mass Ejections During Solar Cycle 23 (1996–2009): Catalog and Summary of Properties, *Solar Phys.*, 264, 189–237, doi:10.1007/s11207-010-9568-6, 2010.
- Richardson, I. G., Cliver, E. W., and Cane, H. V.: Sources of geomagnetic storms for solar minimum and maximum conditions during 1972–2000, *Geophys. Res. Lett.*, 28, 2569–2572, doi:10.1029/2001GL013052, 2001.
- Richardson, I. G., Cane, H. V., and Cliver, E. W.: Sources of geomagnetic activity during nearly three solar cycles (1972–2000), *J. Geophys. Res.*, 107, 1187, doi:10.1029/2001JA000504, 2002.
- Romashets, E. P., Poedts, S., and Vandas, M.: Modeling of the magnetic field in the magnetosheath region, *J. Geophys. Res.*, 113, A02203, doi:10.1029/2006JA012072, 2008.
- Russell, C. T., Luhmann, J. G., Odera, T. J., and Stuart, W. F.: The rate of occurrence of dayside Pc 3,4 pulsations – The L-value dependence of the IMF cone angle effect, *Geophys. Res. Lett.*, 10, 663–666, doi:10.1029/GL010i008p00663, 1983.
- Šafránková, J., Hayosh, M., Gutynska, O., Němeček, Z., and Přech, L.: Reliability of prediction of the magnetosheath  $B_z$  component from interplanetary magnetic field observations, *J. Geophys. Res.*, 114, A12213, doi:10.1029/2009JA014552, 2009.
- Shue, J.-H., Song, P., Russell, C. T., Steinberg, J. T., Chao, J. K., Zastenker, G., Vaisberg, O. L., Kokubun, S., Singer, H. J., Detman, T. R., and Kawano, H.: Magnetopause location under extreme solar wind conditions, *J. Geophys. Res.*, 103, 17691–17700, doi:10.1029/98JA01103, 1998.
- Soucek, J. and Escoubet, C. P.: Predictive model of magnetosheath plasma flow and its validation against Cluster and THEMIS data, *Ann. Geophys.*, 30, 973–982, doi:10.5194/angeo-30-973-2012, 2012.
- Spreiter, J. R., Summers, A. L., and Alksne, A. Y.: Hydromagnetic flow around the magnetosphere, *Planet. Space Sci.*, 14, 223–250, doi:10.1016/0032-0633(66)90124-3, 1966.
- Spreiter, J. R. and Stahara, S. S.: Gasdynamic and magnetohydrodynamic modeling of the magnetosheath: A tutorial, *Adv. Space Res.*, 14, 5–19, doi:10.1016/0273-1177(94)90042-6, 1994.
- Stahara, S. S.: Adventures in the magnetosheath: two decades of modeling and planetary applications of the Spreiter magnetosheath model, *Planet. Space Sci.*, 50, 421–442, doi:10.1016/S0032-0633(02)00023-5, 2002.
- Tatralay, M., Russell, C. T., Luhmann, J. G., Barnes, A., and Mihalov, J. D.: On the proper Mach number and ratio of specific heats for modeling the Venus bow shock, *J. Geophys. Res.*, 89, 7381–7392, doi:10.1029/JA089iA09p07381, 1984.
- Tsyganenko, N. A.: Modeling the Earth's magnetospheric magnetic field confined within a realistic magnetopause, *J. Geophys. Res.*, 100, 5599–5612, doi:10.1029/94JA03193, 1995.
- Tsyganenko, N. A.: Effects of the solar wind conditions in the global magnetospheric configurations as deduced from data-based field models (Invited), *International Conference on Substorms*, ESA Special Publication, 389, Rolfe, E. J. and Kaldeich, B., 181 pp., 1996.
- Turc, L., Fontaine, D., Savoini, P., Hietala, H., and Kilpua, E. K. J.: A comparison of bow shock models with Cluster observations during low Alfvén Mach number magnetic clouds, *Ann. Geophys.*, 31, 1011–1019, doi:10.5194/angeo-31-1011-2013, 2013.
- Walsh, B. M., Sibeck, D. G., Wang, Y., and Fairfield, D. H.: Dawn-dusk asymmetries in the Earth's magnetosheath, *J. Geophys. Res.*, 117, A12211, doi:10.1029/2012JA018240, 2012.
- Wu, C.-C. and Lepping, R. P.: Statistical Comparison of Magnetic Clouds with Interplanetary Coronal Mass Ejections for Solar Cycle 23, *Sol. Phys.*, 269, 141–153, doi:10.1007/s11207-010-9684-3, 2011.
- Yermolaev, Y. I., Nikolaeva, N. S., Lodkina, I. G., and Yermolaev, M. Y.: Geoeffectiveness and efficiency of CIR, sheath, and ICME in generation of magnetic storms, *J. Geophys. Res.*, 117, A00L07, doi:10.1029/2011JA017139, 2012.
- Zhang, J., Liemohn, M. W., Kozyra, J. U., Lynch, B. J., and Zurbuchen, T. H.: A statistical study of the geoeffectiveness of magnetic clouds during high solar activity years, *J. Geophys. Res.*, 109, A09101, doi:10.1029/2004JA010410, 2004.